Universal and Wide Shear Zones in Granular Bulk Flow

Denis Fenistein, Jan Willem van de Meent, and Martin van Hecke

Kamerlingh Onnes Laboratory, Leiden University, P.O. Box 9504, 2300 RA Leiden, The Netherlands

We present experiments on slow granular flows in a modified (split-bottomed) Couette geometry in which wide and tunable shear zones are created away from the sidewalls. For increasing layer heights, the zones grow wider (apparently without bound) and evolve towards the inner cylinder according to a simple, particle-independent scaling law. After rescaling, the velocity profiles across the zones fall onto a universal master curve given by an error function. We study the shear zones also inside the material as a function of both their local height and the total layer height.

                      PACS numbers: 45.70.Mg, 83.50.Ax, 83.85.Cg

Slowly sheared granular matter does not flow homogeneously like a liquid. Instead, granulates form rigid, solidlike regions separated by narrow shear bands where the material yields and flows [1–6]. Shear localization is ubiquitous in granular flow — think of geological faults and soil fractures, avalanches, pipe flows, and silo discharges [2,7–14].

Despite their crucial importance, granular shear flows are still poorly understood, in part because shear localization itself remains enigmatic [1–4]. On the one hand, shear bands have a typical thickness of five to ten grain diameters and such steep gradients are difficult to capture by continuum theories [1–14]. On the other hand, the experimental handles for probing shear localization are limited. For example, studies in Couette cells always show the formation of a narrow shear band near the inner cylinder, irrespective of dimensionality, driving rate, or details of the geometry [5,6,15–18]: Shear banding is very robust.

In this Letter, we introduce a general experimental protocol that can yield very wide shear zones away from the sidewalls. We modify a Couette cell by splitting its bottom at radius R_s. The resulting concentric rings are attached to the stationary inner and rotating outer cylinder, respectively, and the cell is filled with grains up to height H (Fig. 1). When driving the system, a shear zone is found to propagate from the slip position R_s towards the surface where we measure the average grain velocities. Note that our strategy differs from previous works, which were carried out for large filling heights and smooth bottoms so as to minimize the effect of the bottom boundary [5,16,17]. Here we take advantage of gravity and "drive the system from the bottom."

Our main findings are the following: (i) For large H, a regime of wall-localized shear band near the inner cylinder is recovered [5,16,17], but for intermediate H, we observe shear zones of tunable width away from the boundaries. This Letter focuses on describing these "bulk" shear zones. (ii) The angular velocity profiles $\omega(r)$ of bulk shear zones fall onto a universal master curve which is best fitted by an error function. These profiles are therefore fully characterized by two parameters only: their center position R_c and width W. A concise presentation of these results has appeared in [19]. (iii) R_c and W depend on H, R_s, and particle properties in specific manners. The center of the shear zone R_c evolves to the inner cylinder with increasing H in a particle-independent manner. The shear zone width W grows continuously with H and depends on particle size and shape, but not on the slip radius R_s. (iv) For a given height inside the material, the width and position of the shear zones depend on the height of the free surface H.

Setup.—A sketch of our split-bottomed Couette cell is shown in Fig. 1(a). When the inner cylinder of the "Couette" geometry is removed we obtain the "disk" geometry [Fig. 1(b)]. Different sets of bottom rings allow us to vary R_s from 45 to 95 mm. Grains, similar to those used in the bulk, are glued to the sidewalls and bottom rings to obtain rough boundaries. We studied spherical glass beads of size distributions 0.25–0.42 mm (I), 0.5–0.8 mm (II), 1–1.2 mm (III), and 2–2.4 mm (IV), and irregularly shaped plastic flakes (1.0–1.6 mm) (V), aluminum oxide beads (1.5–2 mm) (VI), and coarse sand (1.2–2.4 mm) (VII). After filling the cell, an adjustable
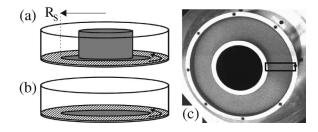
FIG. 1. (a) Schematic side-view of our split-bottomed Couette cell, showing the stationary bottom disk and inner cylinder (both gray), and the rotating bottom ring (striped) and outer cylinder. A thin layer of felt between the rings assures smooth rotation. The inner and outer cylinder radii are fixed at 65 and 105 mm, respectively, while R_s can be varied. (b) Setup in disk geometry. (c) Top view of the filled set up in the Couette geometry, where the rectangle indicates the area recorded by the video camera.

blade flattens the surface at the desired height. The outer cylinder and its comoving ring are then rotated. A Pulnix TM-6710 8-bit CCD camera records 2000-frame movies of the resulting flow at the top surface at a rate of 120 frame/s with pixel resolution 100 μm.
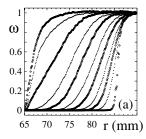
The flow rapidly (~ 1 s) reaches a stationary state where it is purely in the azimuthal direction, so that the surface velocities are a function of the radial coordinate only [5,6,15–17,19]. We checked that these velocities are proportional to the driving rate Ω [5,16,18,19] for $0.16 < \Omega < 1.5$ rad/s, and subsequently fix Ω at 0.16 rad/s. We thus focus on the velocity profile $\omega(r)$, the dimensionless ratio of the average angular velocity, and Ω. We measure $\omega(r)$ with high radial resolution by particle image velocimetry, i.e., by determining the averaged angular correlation function as function of r of two temporally separated frames. Unless noted otherwise, the time separation between frames is around 0.3 s.

Basic phenomenology.—Figure 2 illustrates the main features of these velocity profiles. For shallow layers, a narrow shear zone develops above the split at R_s. When H is increased, the shear zone broadens continuously and without any apparent bound. The broadest observed zones exceed 50 grain diameters in width. Additionally, with increasing H, the shear zone shifts away from R_s towards the center of the shear cell [20]. Indeed, for sufficiently large H, the shear zone reaches the inner wall, where it approaches the asymptotic regime of wall-localized shear bands reported earlier [5,16,17]. Before this wall localization occurs, however, there is a substantial range of layer heights where wide and symmetric bulk shear zones can be observed.

Universal velocity profiles.—Figure 3 illustrates our main result: After proper rescaling, all bulk profiles collapse on a universal curve which is extremely well fitted by an error function:

$$\omega(r) = 1/2 + 1/2 \, \text{erf}[(r - R_c)/W]. \quad (1)$$

A residue analysis comparing the fit to Eq. (1) to an alternative fit to an hyperbolic tangent shows that the fit to the error function is always better [Fig. 3(b) and 3(c)]. By repeating this procedure for the other particle mixtures, we establish the general superiority of Eq. (1): *particle shape does not influence the functional form of the velocity profiles.* The robust form of $\omega(r)$ contrasts with the particle dependence found for wall-localized shear bands [5]. For these, the vicinity of the wall causes layering, in particular, for monodisperse mixtures. Apparently such layering effects play no role for our bulk shear zones. Accurate measurement of the tail of the velocity profile [Fig. 3(d)] further validate Eq. (1), and rule out an exponential tail of the velocity profile here. The strain rate is therefore Gaussian, and the shear zones are completely determined by their centers R_c and widths W.

What limits the universal regime? Apart from wall localization (see Fig. 2), we find that in the disk geometry $\omega(r)$ starts to deviate from Eq. (1) when H exceeds $\sim R_s/2$. The symmetry of the velocity profile, easily detectable by a simple χ^2 test, is then weakly broken [21]. In the following, we focus on the functional dependencies of R_c and W on the parameters R_s, H, and particle type for the universal profiles given by Eq. (1).

Shear zone position.—Remarkably, the shear zone center evolution with height $R_c(H)$, turns out to be independent of the grain properties [Fig. 4(a)]. Therefore, the only relevant length scales for R_c are the geometric scales H and R_s. The dimensionless displacement of the shear zone, $(R_s - R_c)/R_s$, should thus be a function of the
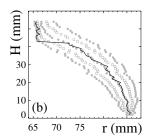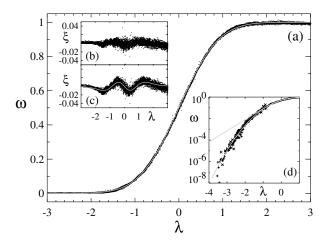

FIG. 2. Main features of the normalized angular surface velocity in the Couette geometry for 0.3 mm glass beads (mixture I) and $R_s = 85$ mm. (a) $\omega(r)$ for a range of equidistant heights $h = 3, 8, \ldots, 53$ mm (right to left). (b) Contour plots of $\omega(r)$, where the symbols correspond to, from left to right, $\omega = 0.1, 0.25, 0.5, 0.75$, and 0.9. The curve indicates the strain rate maximum and shows the rapid qualitative change of the profiles when the inner cylinder is approached.

FIG. 3. (a) Collapse of all 35 bulk profiles obtained for $H = 4, 5, 6, \ldots, 38$ mm (mixture I, $R_s = 85$ mm, as in Fig. 2) when plotted as function of the dimensionless coordinate $\lambda := (r - R_c)/W$. The gray curve is an error function. (b) Differences ξ between bulk profiles and fits to Eq. (1). (c) Differences ξ between bulk profiles and fits to $1/2 + 1/2 \tanh(l\lambda)$, where $l \approx 1.202\,74$ compensates for the difference in scale between error function and hyperbolic tangent. The gray curve shows $[\text{erf}(\lambda) - \tanh(l\lambda)]/2$. (d) Left tail of the velocity profile in loglin scale, compared to the best fit to either a hyperbolic tangent and error function (gray curves). Dots, crosses, and plusses are obtained for time lags 0.3, 3, and 30 s, respectively.
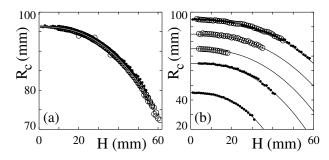
FIG. 4. Shear zone positions R_c versus height, where H is restricted to the universal regime detected by a χ^2 test. (a) Comparison between $R_c(H)$ for glass beads I-IV (closed symbols), nonspherical particles V-VII (open symbols) and Eq. (2) (curve). For all runs, R_s is 95 mm. (b) $R_c(H)$ for mixture III and $R_s = 95$, 85, and 75 mm in the Couette geometry (open symbols) and $R_s = 95$, 65, and 45 mm in the disk geometry (closed symbols), compared to Eq. (2) (curves).

dimensionless height (H/R_s) only. The simple relation

$$(R_s - R_c)/R_s = (H/R_s)^{5/2} \qquad (2)$$

fits the data well [Fig. 4(a)] [22]. To check Eq. (2) we have varied R_s over a substantial range. Only the presence of the inner cylinder limits the range of R_s. We find no differences between bulk velocity profiles measured with or without the inner cylinder—*Bulk shear zones are insensitive to the presence of the sidewalls.* So, we subsequently switched to the disk geometry [Fig. 1(b)], and obtained an excellent agreement between R_c and Eq. (2) over the range $45 < R_s < 95$ mm [Fig. 4(b)].

Shear zone width.—The width of the shear zones depends on the particle size and type [Figs. 5(a)–5(c)], but not on R_s [Fig. 5(d)]. First of all, W grows with H and increases for larger particles [Figs. 5(a) and 5(b)]. The data shown in Figs. 5(a) and 5(b) can be made to collapse when plotted as W/d vs H/d (not shown), where d denotes the grain size. Grain shape and type also influences $W(H)$: irregular particles display narrower zones than spherical ones of similar diameter [Fig. 5(c)]. Finally, for the universal velocity profiles, W is independent of R_s [Fig. 5(d)]. We therefore conclude that the relevant length scale for W is given by the grain properties.

The evolution of the velocity profiles from a step function at the bottom to an error function at the surface, is reminiscent of a diffusive process along the vertical axis. However, W grows faster than $\sqrt{H}$ as diffusion would suggest, but slower than H. Intriguingly, we obtain the best fit for $W \propto H^{2/3}$ over the limited range where we have reliable data. We cannot, however, rule out other functional dependencies such as a crossover from square-root to linear behavior.

Below the surface—So far we have only discussed observations of the surface flow. To get some insight into the 3D bulk flow structure, we put patterns of lines of colored tracer particles at given H_b [Fig. 6(a)]. More
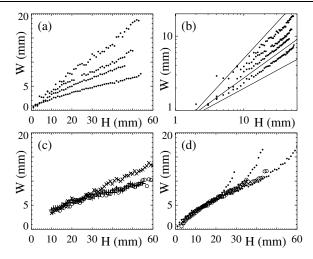

FIG. 5. Width of the shear zones versus H. (a) Linear and (b) log-log plots of W for spherical glass beads of increasing sizes for $R_s = 95$ mm (mixture I-IV). The width grows with particle size. The straight lines in (b) have slopes 1/2, 2/3, and 1, showing that W grows faster than $\sqrt{H}$ but slower than H. (c) Irregular particle shapes diminish W substantially, as can be seen by comparing the widths for the plastic flakes (V/pluses), aluminum oxide beads (VI/open circles), and coarse sand (VII/crosses) to those of the glass beads shown in panel (a). (d) W for mixture III and $R_s = 95$, 85, and 75 mm (Couette geometry; open symbols) and $R_s = 95$, 65, and 45 mm (disk geometry; closed symbols). The strong upward deviations observed in the disk geometry coincide with the symmetry breaking of the velocity profiles (see text). Apart from this, the setup geometry does not affect W.

material is carefully added so that the line pattern is buried under a given amount of grains ($H > H_b$). We then rotate the system for a short period (~ 8 s), and recover the deformed line pattern by carefully removing the upper layers of grains [Fig. 6(b)]. Comparing the snapshots of the deformed pattern to the initial one allows for the determination of the velocity profiles *in the 3D bulk of the material* [Fig. 6(c)]. We have checked that transient effects are limited, that the measurements reproduce well and that there is no significant motion in the vertical direction.

The position of the shear zones in the 3D bulk are presented in Fig. 6(d). Clearly, the evolution of R_c with H_b inside the material depends on the total amount of matter, as given by H: the more material added, the more the shear zone shifts towards the center. This observation is confirmed by recent theory [23], numerics [24], and MRI measurements [25]. The widths of the 3D shear zones are more difficult to measure accurately, but a clear trend can be identified: shear zones become wider when more matter is added on top [Fig. 6(e)].

Outlook—In this Letter we have presented a simple experimental protocol in which wide and tunable shear zones can be generated in a variety of granular materials. Perhaps the biggest surprise is the robust and remarkably simple form of the velocity profiles—for granular
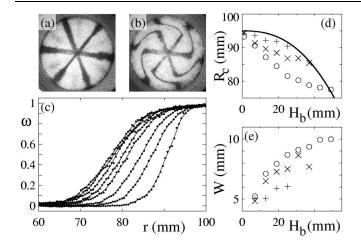
FIG. 6. Measurements of $\omega(r)$ inside the material for the disk geometry and $R_s = 95$ mm. (a) Initial pattern at $H_b = 31$ mm. (b) The same pattern after adding material up to $H = 49$ mm, rotating, and removing the upper layers. (c) Velocity profiles for $H = 49$ mm, and $H_b = 7, 13, 19, \ldots, 49$ mm (from right to left). (d) $R_c(H_b)$ for $H = 25$ mm (plusses), $H = 37$ mm (crosses), and $H = 49$ mm (circles) compared to $R_c(H)$ given by Eq. (2) (curve). (e) Corresponding $W(H_b)$.

systems, universality is rare. Our measurements of the tail of the profile indicate that even far away from the shear zone, the grains are not entirely at rest. These findings indicate that these features are amenable to a continuum description of granular matter [1–4], in particular, for very wide shear zones.

It is also noteworthy that the functions for the shear zone location $R_c(H)$ and width $W(H)$ depend on entirely distinct sets of parameters: the relevant length scales for R_c and W appear to be well separated. The particle dependence of the width provides a characteristic length scale which may bridge microscopic and coarse-grained descriptions. The development of theories of granular flows can further be guided by the universal relation for the shear zone position, and should incorporate the strong influence of the boundary: Avoiding the proximity of the side wall can turn the shear zones from narrow to wide, and from particle dependent to universal.

The broad shear zones occurring in our geometry allow for further experiments that are more difficult to realize in narrowly localized shear bands. Important issues can thus be tackled, such as the velocity fluctuations and particle diffusion for various strain rates and locations within the shear zone. One can also probe whether "local clusters" of particles, possibly similar to those found in more rapid flows, would occur for these denser flows [26]. Finally, over the range studied, the velocity profiles are rate independent, but what happens for much larger and smaller rotation rates is an open question. The simple experimental protocol that we provide for creating generic (i.e., away from sidewalls) shear zones can be the starting point for many crucial experiments, thus addressing the basic question: "How does sand flow?"

[1] J. Duran, *Sand, Powders and Grains* (Eyrolles, Paris, 1997).
[2] R. Nedderman, *Statics and Kinematics of Granular Materials* (Cambridge University Press, Cambridge, United Kingdom, 1992).
[3] H. M. Jaeger, S. R. Nagel, and R. P. Behringer, Rev. Mod. Phys. **68**, 1259 (1996).
[4] H. M. Jaeger and S. R. Nagel, Science **255**, 1523 (1992).
[5] D. M. Mueth, *et al.* Nature (London) **406**, 385 (2000).
[6] R. R. Hartley and R. P. Behringer, Nature (London) **421**, 928 (2003).
[7] D. R. Scott, Nature (London) **381**, 592 (1996).
[8] M. Oda and H. Kazama, Géotechnique **48**, 465 (1998).
[9] J. Bridgewater, Géotechnique **30**, 533 (1980).
[10] H. B Muhlhaus and I. Vardoulakis, Géotechnique **37**, 271 (1987).
[11] T. S. Komatsu, S. Inagaki, N. Nakagawa, and S. Nasuno, Phys. Rev. Lett. **86**, 1757 (2001).
[12] A. Daerr and S. Douady, Nature (London) **399**, 241 (1999).
[13] O. Pouliquen and R. Gutfraind, Phys. Rev. E **53**, 552 (1996).
[14] R. M. Nedderman and C. Laohakul, Powder Technol. **25**, 91 (1980).
[15] D. Howell, R. P. Behringer, and C. Veje, Phys. Rev. Lett. **82**, 5241 (1999).
[16] W. Losert, L. Bocquet, T. C. Lubensky, and J. P. Gollub, Phys. Rev. Lett. **85**, 1428 (2000).
[17] W. Losert and G. Kwon, Adv. Complex Syst. **4**, 369 (2001).
[18] M. Lätzel, S. Luding, H. J. Herrmann, D.W. Howell, and R. P. Behringer, Eur. Phys. J. E **11**, 325 (2003).
[19] D. Fenistein and M. van Hecke, Nature (London) **425**, 256 (2003).
[20] For an essentially 2D flow, i.e., stratified and far away from the bottom, the shear stresses increase for decreasing radius [18]. Presumably, for deep enough layers a related mechanism pulls the shear zones inward.
[21] Note that an asymmetric correction to Eq. (1) also occurs when one assumes that the shear rate $\dot{\gamma}(r)$ is strictly symmetric (Gaussian), and calculates $\omega(r)$ as $\int r\dot{\gamma}(r)dr$. This correction to Eq. (1) is, however, negligibly small for our values of H and R_s, so we have ignored it here. More importantly, such correction grows continuously with H, rather than suddenly appearing at $H \approx R_s/2$.
[22] We found some indications that strongly elliptical grains (birdseed/not presented here) deviate from Eq. (2).
[23] T. Unger, J. Török, J. Kertész, and D. E. Wolf, cond-mat/0401143.
[24] S. Luding (private communications).
[25] P. Umbanhowar (private communications).
[26] D. Bonamy, F. Daviaud, L. Laurent, M. Bonetti, and J. P. Bouchaud, Phys. Rev. Lett. **89**, 034301 (2002).